



Phase identification and morphology in rolled and annealed U-22.5at.%Zr foils

Walter J. Williams^{1,2} · Tiankai Yao² · Laura Sudderth² · Fidelma Di Lemma² · Luca Capriotti² · Maria A. Okuniewski¹

Received: 16 September 2021 / Accepted: 4 November 2021 / Published online: 24 November 2021
© The Author(s), under exclusive licence to The Materials Research Society 2021

Abstract

A uranium-22.5 atomic% zirconium (U-22.5at.%Zr) alloy was characterized using transmission electron microscopy (TEM) following hot/cold-rolling, and again following a post-roll anneal as part of a novel fabrication process for the alloy. The TEM characterization included selected area electron diffraction, energy-dispersive X-ray spectroscopy (EDS), and bright field imaging. The δ -UZr₂ phase fraction was $53.47\% \pm 0.09\%$ in the rolled foil, substantially larger than the near-equilibrium value, $21.93\% \pm 0.03\%$ in the annealed foil. Phase fractions and EDS analysis suggest a defect-driven U supersaturation in the δ -UZr₂ phase. The lamellae mean random spacing was $0.21 \mu\text{m} \pm 0.03 \mu\text{m}$ in the rolled foil and $0.70 \mu\text{m} \pm 0.10 \mu\text{m}$ in the annealed foil. The δ -UZr₂ L₃ values were $0.11 \mu\text{m} \pm 0.02 \mu\text{m}$ in the rolled foil and $0.16 \mu\text{m} \pm 0.03 \mu\text{m}$ in the annealed foil. Zirconium inclusions in all foils were face-centered cubic (space group Fm-3 m), reinforcing that further investigations into the formation mechanism(s) and evolution of Zr inclusions are needed.

Introduction

During reactor operation, the uranium-22.5 atomic% zirconium (U-22.5at.%Zr) system nominally operates between 500 and 700 °C with thermal gradients near 35 °C/mm, and the peak temperature at the center of the cylindrical fuel [1, 2]. The primary phenomena impacting the alloy under these reactor conditions include fuel-cladding chemical interaction, fuel swelling, fuel-cladding mechanical interactions, and constituent redistribution [3–8]. These phenomena are impacted by material properties, such as heat of transport and diffusivity, which are in turn dictated by crystal structure and phase morphology [9–12]. Due to the harsh reactor environment, in situ crystallographic and morphological studies are non-existent, therefore relying on pre- and post-irradiation experiments to comprehend the microstructural evolution of the fuel.

While the equilibrium U–Zr phase diagram is best described by Rough and Bauer [13, 14], there is room for furthering the fundamental understanding [15–17] to

ensure that novel fabrication techniques result in a known microstructure. Typically fabricated (i.e., cast, extruded, and annealed) U-22.5at.%Zr fuel observed at room temperature is comprised of a binary structure of α -U (Cmcm), with < 1at.%Zr solubility [18, 19], and δ -UZr₂ (P6/mmm), with a composition of U-66.3at.%Zr [23], with Zr inclusions dispersed throughout the matrix [13–15, 20–22]. The morphology of the α -U and δ -UZr₂ phases is determined by composition, fabrication methods, and cooling rates [23, 24], whereas the Zr inclusions remain relatively unaffected by heat treatments [15]. As the initial microstructure may impact phase and crystallographic evolution in a reactor [3], characterization should be performed on each uniquely fabricated U–Zr alloy.

This study characterizes the un-irradiated microstructure of U-22.5at.%Zr fuel foils intended for separate effects irradiation testing, which enables the deconvolution of reactor power, temperature, and composition using unique irradiation vehicle designs and fuel geometries [25–27]. Two types of foils were investigated, including a heavily rolled fuel foil and an annealed (following rolling) fuel foil. Rolling and subsequent heat treating is a novel fabrication technique for U–Zr alloys, requiring characterization to quantify microstructural differences and recovery. Characterization via transmission electron microscopy (TEM) and stereological methods included crystal structure and phase identification, as well as morphological quantification.

✉ Walter J. Williams
Walter.Williams@inl.gov

¹ School of Materials Engineering, Purdue University, 701 West Stadium Ave. ARMS, West Lafayette, IN 47907, USA

² Idaho National Laboratory, MFC-1742, Scoville, ID 83415-0001, USA

Materials and methods

A U-22.5at.%Zr ingot was drop cast via arc-melting into a Cu mold in an inert atmosphere glovebox [15, 25]. Sample-A was harvested with a focused ion beam from a foil, fabricated by hot-rolling to a ~90% reduction, annealing for two hours at 800 °C, then cold-rolling to a final ~60% reduction of the ingot. Samples-B,C were harvested from the same foil following a two-hour anneal, after rolling, at 900 °C with a 1 °C/min cooling rate.

TEM bright field (BF) images, dark field (DF) images, and energy-dispersive X-ray spectroscopy (EDS) maps were collected (200 kV accelerating voltage) on all samples using a FEI Titan ChemiSTEM FEG-STEM. Selected area electron diffraction (SAED) was performed on various regions and analysis was completed using manual measurements in conjunction with CrysTBox [28]. Stereology was performed following methods described by Underwood [29] and Vander Voort [30]. Further details can be found in the Supplementary Materials.

Results

Sample-A has two major U–Zr phases, a U-rich phase and a Zr-rich phase as pictured in Fig. 1c, d, j, k, l, in a lamellar structure and one minor phase, Zr inclusions, as pictured in Fig. 1a, b. No minor elements were detectable, using EDS, in the bulk material of Samples-A, C. Figure 1j, k, l, shows a compositional gradient in the Zr-rich phase, with Zr content increasing from 15at.%Zr near the phase boundary to 63at.%Zr in the center. Figure 1j, k, l also shows that the U-rich portion of the lamellar structure has a consistent composition near U-15at.%Zr. The SAED patterns, Fig. 1f, h, identify the Zr-rich phase to be space group of P6/mmm (hexagonal δ -UZr₂ [31]), and the U-rich phase to be space group of Cmcm (orthorhombic α -U [32]). The SAED patterns of δ -UZr₂ and α -U show nanocrystalline grains in the bulk microstructure, indicated by the onset of rings in Fig. 1f, h. The δ -UZr₂ and α -U lamellar structures are morphologically distorted near the minor phase, Fm-3 m (face-centered cubic, FCC) Zr inclusions, indicated by Fig. 1b, g, i. Line scans across the Zr inclusions, Fig. 1j, k, indicate a composition of U-85at.%Zr.

Figure 2a–g shows that Samples-B,C have the same phases, α -U [32] and δ -UZr₂ [31] and dispersed inclusions, with a broadened and coarsened lamellar structure, as compared to Sample-A. The EDS line scans across the lamellar structure, Fig. 2h, i, j, shows that the Zr-rich phase has a composition near U-63at.%Zr and the U-rich phase has a composition near U-15at.%Zr, in agreement with Sample-A.

The SAED patterns of the δ -UZr₂ and α -U structure following the annealing, Fig. 2f, g, show no evidence of reorientation or nanocrystalline grains, which were present following rolling. The line scan in Fig. 2i indicates the inclusions in Sample-B remain near U-85at.%Zr. SAED of the Zr inclusions in Sample-C, shown in Fig. 2k, l, m, n, confirms that the Zr inclusion remains as Fm-3m following annealing.

Stereology results for Samples-A, B include volume fraction (V_V , measured as P_P), features per line (N_L), and the mean intercept length, L_3 , and mean random spacing, σ_r , between lamellae are presented in Table 1. The phase fraction (P_P) for δ -UZr₂ in Sample-A, is greater than twice that of Sample-B. Inclusions in the rolled Sample-A are more prevalent; however, sample population is limited by sample size relative to bulk microstructure. The L_3 and σ_r values verify a finer lamellar structure in Sample-A than observed in Sample-B, which has a broader and coarser lamellar structure.

Discussion

All foils were comprised of two primary phases, δ -UZr₂ [31] and α -U [32], in a lamellar structure. The lamellar structure in Sample-B lacks indications of reorientation or nano-grains observed in Sample-A, agreeing with expected results following a 900 °C anneal [15, 24]. Sample-B has a mean random spacing between lamellae over three times that of rolled Sample-A, appears coarsened, and increasingly globular. The differences in the lamellar formation and coarsening is expected to be due to different cooling rates between hot-rolling and annealing as well as deformation induced during rolling [24].

The EDS results of all samples show a semi-quantitative composition in α -U, near 15at.%Zr, measuring higher than the literature value, < 1at.%Zr solubility [18]. The δ -UZr₂ phase in Sample-B was measured to be UZr₂ at 63at.%Zr, indicating that the high Zr solubility in α -U is non-negligible. The EDS results of δ -UZr₂ in Sample-B show the Zr content plateauing near the phase boundary interfaces. In contrast, the δ -UZr phase in Sample-A shows a compositional gradient, also peaking near 63at.%Zr in the center of the phase. While the peak composition of both samples is the same, the compositional plateauing was not apparent in the Sample-A. Although the electron interaction volume was consistent for all samples, at ~50–100 nm³, the finer lamellar structure in Sample-A could result in an oversampling of lamella co-located within the thickness of the sample (~50 nm), thus causing the compositional disparity, or supersaturation of U in the δ -UZr phase, to be difficult to quantify.

However, increasing U in the δ -UZr₂ phase also results in differing phase fractions between Samples-A,B. Sample-B, comprised of $76.32\% \pm 0.02\%$ α -U, $21.93\% \pm 0.03\%$ δ -UZr₂, and $1.75\% \pm 0.03\%$ Zr inclusions, is in near agreement with the equilibrium system [13, 14, 33]. Sample-A, comprised of $41.99\% \pm 0.07\%$ α -U, $53.47\% \pm 0.09\%$ δ -UZr₂, and $4.53\% \pm 0.05\%$ Zr inclusions, differs significantly from the equilibrium system, indicating the supersaturation of U in deformed δ -UZr₂. Further investigation into the relationship between defect concentration and phase fractions in U–Zr is of interest since the nuclear fuel is subjected to a defect-producing environment. This is particularly important since phases determine bulk behavior [9, 10].

Inclusions in U-22.5at.%Zr alloys have been both hypothesized and measured to be α -Zr (hexagonal close-packed, HCP) stabilized by a minor constituent, such as O or N [5, 34, 35], typically originating from the Zr-rind on the edge of a casting [36]. Alternate findings suggest that the Zr inclusions may form during solidification [37] and result in an FCC structure, hypothesized to be caused by unknown differences in casting techniques [38]. The Zr inclusions in this

study were found to be FCC, rather than HCP α -Zr. The first observation of an HCP to FCC transformation in Zr was made in 2002 during ball-mill mechanical attrition of pure Zr [39] and again in 2017 during the cold-rolling of pure Zr [40]. Therefore, additional research is needed to determine whether the FCC structure was present due to the casting technique or if the inclusions underwent a stress-induced phase transformation during cold-rolling.

Conclusions

TEM-SAED indexing, TEM-EDS analysis, and stereology were used to quantify the microstructure of U-22.5at.%Zr samples following a novel fabrication process of rolling and annealing. A sample was characterized following hot- and cold-rolling. Two additional samples were characterized following a post-roll anneal. The rolled sample had a supersaturation of U in the δ -UZr₂ phase, resulting in a phase fraction of δ -UZr₂ more than twice that of the equilibrium system. This finding suggests that the defect concentration

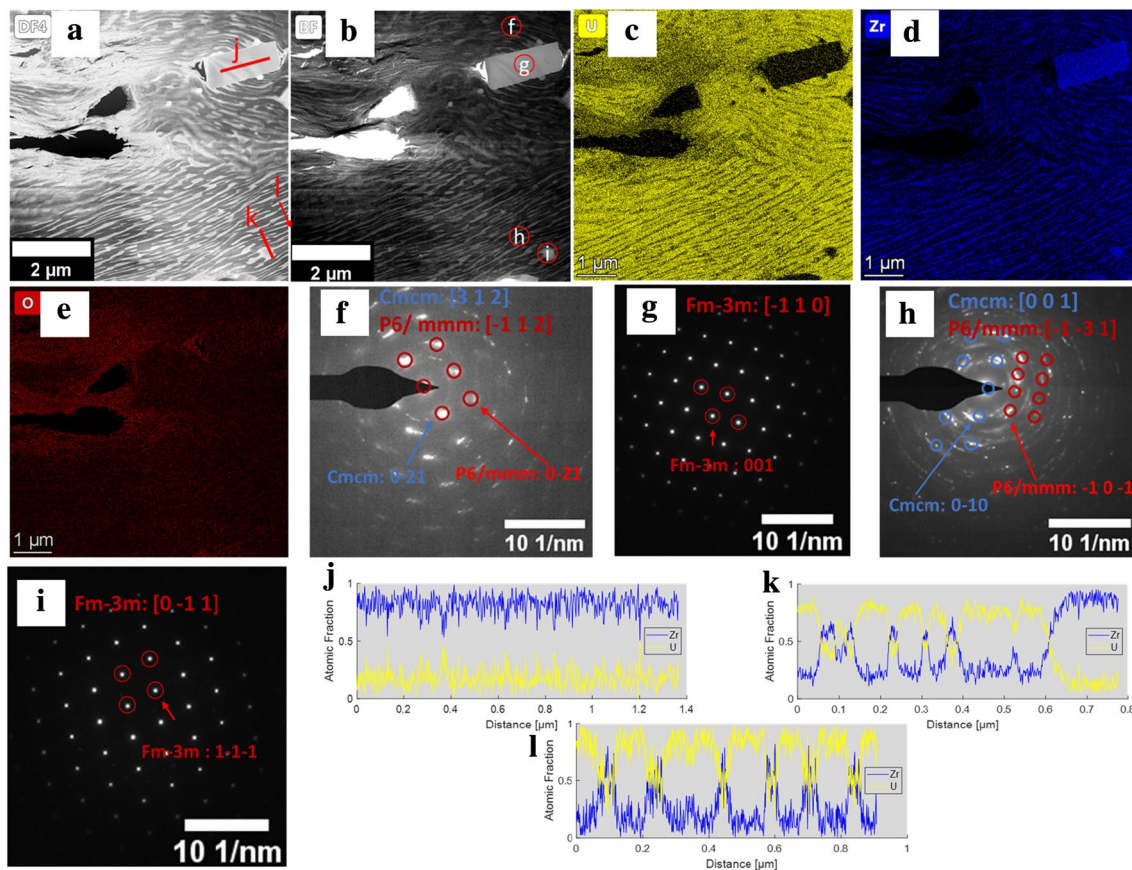


Fig. 1 Heavily rolled U-22.5at.%Zr foil, Sample-A, showing: (a) Dark field TEM image with the locations of EDS line scans (red) corresponding to subfigures j–l. (b) Bright field TEM image with red SAED locations corresponding to diffraction patterns f–i. EDS maps

of (c) U, (d) Zr, and (e) O. (f,g,h,i) SAED patterns with the zone axis and diffraction spots indicated. The locations of the patterns collected are indicated with the corresponding figure labels in (b). (j, k, l) EDS line scans of U and Zr corresponding to locations in (a)

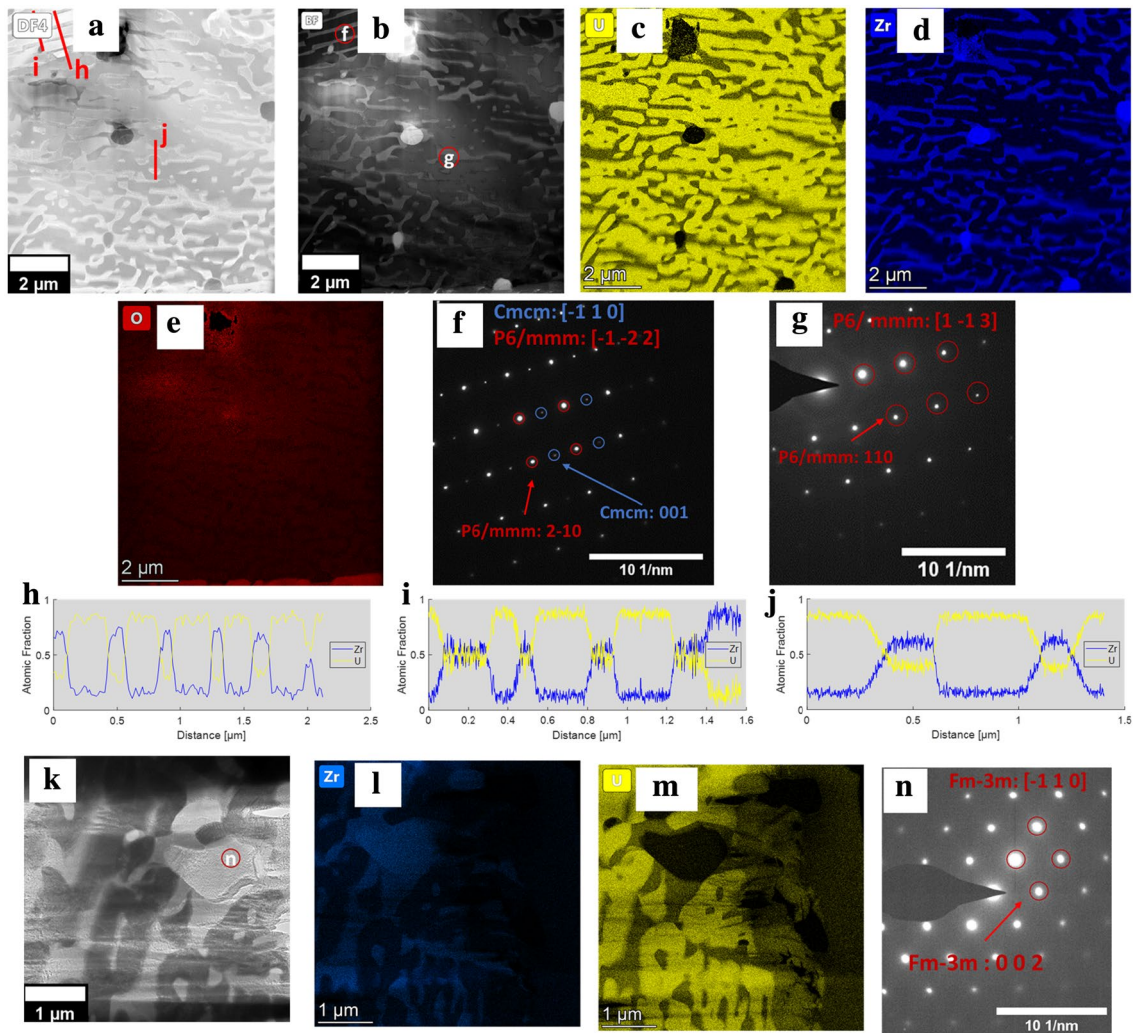


Fig. 2 Samples-B,C, U-22.5at.%Zr foils annealed at 900 °C for two hours followed by a 1 °C/min cooling rate. (a) Dark field TEM image of Sample-B with the locations of EDS line scans (red) corresponding to figures h–j. (b) Bright field TEM image with red SAED locations corresponding to diffraction patterns f and g. EDS maps of (c) U. (d) Zr. (e) O. (f–g) SAED patterns with the zone axis and diffrac-

tion points indicated on each figure. (h–j) EDS line scans corresponding to figure a, with Zr (blue) and U (yellow). (k) Dark field TEM image of Zr inclusion in Sample-C with red circle corresponding to the SAED in (n). EDS maps of (l) Zr. (m) U. (n) SAED pattern of Zr inclusion with the zone axis and diffraction points indicated

of the alloy may have a higher impact on the microstructural evolution and Zr migration within the fuel than is commonly thought. Inclusions in the sample were FCC Zr, rather than HCP α -Zr, reinforcing the need for further studies on the formation and evolution of Zr inclusions to identify the mechanisms that determine the crystal structure.

The annealed sample was found to be in close agreement with the equilibrium system, typically fabricated by casting, extrusion, and heat treatment. Following annealing, the phase fractions returned to expected values predicted by the phase diagram of 21.93% \pm 0.03% δ -UZr₂ and 76.32% \pm 0.02% α -U with dispersed FCC Zr inclusions.

Table 1 Stereology results for Samples-A,B, including: (a) the volume fraction for each phase, P_p , using 300 randomly located points per image, (b) the number of features per line, N_L , or the number of

phase intercepts per μm of random test lines, (c) the mean intercept length for the δ -UZr₂ phase, $L_3 = P_p/N_L$ [32], and (d) the mean random spacing between lamellae, $\sigma_r = 1/N_L$ [33]

Sample	$V_V \delta\text{-UZr}_2$ [%]	$V_V \alpha\text{-U}$ [%]	V_V inclusions [%]	$L_3 = P_p\text{-}\delta\text{-UZr}_2/N_L$ [μm]	$\sigma_r = 1/N_L$ [μm]
A (rolled)	53.47 \pm 0.09	41.99 \pm 0.07	4.53 \pm 0.05	0.11 \pm 0.02	0.21 \pm 0.03
B (annealed)	21.93 \pm 0.03	76.32 \pm 0.02	1.75 \pm 0.03	0.16 \pm 0.03	0.70 \pm 0.10

These findings show that post-rolling heat treatments can recover U–Zr fuel microstructures found in traditionally cast fuel slugs [20] with lamellar spacing dependent upon heat treatments.

In both samples, the solubility of Zr in α -U was identified to be higher, 15at.%, than the values historically reported. While this is not an absolute measurement of Zr solubility, it does represent the need for further studies, such as atom probe tomography, where precise quantification can be performed.

Supplementary Information The online version contains supplementary material available at <https://doi.org/10.1557/s43580-021-00162-6>.

Acknowledgements This research was partially supported by the US Department of Energy, Office of Nuclear Energy (NE), under DOE Idaho Operations Office Contract DE-AC07-05ID14517 through a Nuclear Science User Facilities experimental project and the Advanced Fuel Campaign. TEM Characterization took place in the Irradiated Material Characterization Laboratory at Idaho National Laboratory.

Data availability The datasets generated during and/or analyzed during the current study are not publicly available beyond what is included in this publication due to being included in an ongoing PhD program. However, the data may be made available from the corresponding author on reasonable request.

Declarations

Conflict of interest On behalf of all authors, the corresponding author states that there is no conflict of interest.

References

- W.J. Carmack, H.M. Chichester, D.L. Porter, D.W. Wootan, Metallography and fuel cladding chemical interaction in fast flux test facility irradiated metallic U-10Zr MFF-3 and MFF-5 fuel pins. *J. Nucl. Mater.* **473**, 167–177 (2016). <https://doi.org/10.1016/j.jnucmat.2016.02.019>
- J.M. Harp, D.L. Porter, B.D. Miller, T.L. Trowbridge, W.J. Carmack, Scanning electron microscopy examination of a Fast Flux Test Facility irradiated U-10Zr fuel cross section clad with HT-9. *J. Nucl. Mater.* **494**, 227–239 (2017). <https://doi.org/10.1016/j.jnucmat.2017.07.040>
- W.J. Williams, D.M. Wachs, M.A. Okuniewski, S. van den Berghe, Assessment of swelling and constituent redistribution in uranium-zirconium fuel using phenomena identification and ranking tables (PIRT). *Ann. Nucl. Energy.* **136**, 107016 (2020). <https://doi.org/10.1016/j.anucene.2019.107016>
- C. Matthews, C. Unal, J. Galloway, D.D. Keiser, S.L. Hayes, Fuel-cladding chemical interaction in U-Pu-Zr metallic fuels: a critical review. *Nucl. Technol.* **198**, 231–259 (2017). <https://doi.org/10.1080/00295450.2017.1323535>
- Y.H. Sohn, M.A. Dayananda, G.L. Hofman, R.V. Strain, S.L. Hayes, Analysis of constituent redistribution in the γ (bcc) U-Pu-Zr alloys under gradients of temperature and concentrations. *J. Nucl. Mater.* **279**, 317–329 (2000). [https://doi.org/10.1016/S0022-3115\(99\)00290-1](https://doi.org/10.1016/S0022-3115(99)00290-1)
- G.L. Hofman, S.L. Hayes, M.C. Petri, Temperature gradient driven constituent redistribution in U-Zr alloys. *J. Nucl. Mater.* **227**, 277–286 (1996). [https://doi.org/10.1016/0022-3115\(95\)00129-8](https://doi.org/10.1016/0022-3115(95)00129-8)
- G.L. Hofman, R.G. Pahl, C.E. Lahm, D.L. Porter, Swelling behavior of U-Pu-Zr fuel. *Metall. Trans. A* **21**, 517–528 (1990). <https://doi.org/10.1007/BF02671924>
- R.G. Pahl, D.L. Porter, C.E. Lahm, G.L. Hofman, Experimental studies of U-Pu-Zr fast reactor fuel pins in the experimental breeder reactor-II. *Metall. Trans. A* **21**, 1863–1870 (1990). <https://doi.org/10.1007/BF02647233>
- N.N. Carlson, C. Unal, J.D. Galloway, Formulation of the Constituent Distribution Model Implemented into the BISON Framework for the Analysis of Performance of Metallic Fuels with Some Initial Simulations Results, Los Alamos Natl. Lab. Rep. LAUR 13-26 (2013)
- J.D. Hales, R.L. Williamson, S.R. Novascone, G. Pastore, B.W. Spencer, D.S. Stafford, K.A. Gamble, D.M. Perez, R.J. Gardner, W. Liu, J. Galloway, C. Matthews, C. Unal, N. Carlson, BISON Theory Manual The Equations Behind Nuclear Fuel Analysis, INL/EXT-13-29930 Rev. 3 (2016)
- J. Galloway, C. Unal, N. Carlson, D. Porter, S. Hayes, Modeling constituent redistribution in U-Pu-Zr metallic fuel using the advanced fuel performance code BISON. *Nucl. Eng. Des.* **286**, 1–17 (2015). <https://doi.org/10.1016/j.nucengdes.2015.01.014>
- R.R. Mohanty, J. Bush, M.A. Okuniewski, Y.H. Sohn, Thermotransport in γ (bcc) U-Zr alloys: a phase-field model study. *J. Nucl. Mater.* **414**, 211–216 (2011). <https://doi.org/10.1016/j.jnucmat.2011.03.028>
- A.A. Bauer, G.H. Beatty, F.A. Rough, R.F. Dickerson, Constitution of Zirconium-Uranium Alloys Containing Oxygen or Nitrogen, Battelle Meml. Inst. BMI-1187 (1957)
- F.A. Rough, A.A. Bauer, Constitution of uranium and thorium alloys, Battelle Meml. Inst. BMI-1300 (1958)
- W.J. Williams, M.A. Okuniewski, S.C. Vogel, J. Zhang, An in-situ neutron diffraction study of crystallographic evolution and thermal expansion coefficients in U-22.5at.%Zr during annealing. *JOM* **72**, 2042–2050 (2020). <https://doi.org/10.1007/s11837-020-04086-8>
- Y. Xie, S.C. Vogel, J.M. Harp, M.T. Benson, L. Capriotti, Microstructure evolution of U-Zr system in A thermal cycling neutron diffraction experiment: extruded U-10Zr (wt.%). *J. Nucl. Mater.* **544**, 152665 (2021). <https://doi.org/10.1016/j.jnucmat.2020.152665>
- S. Ahn, S. Irukuvarghula, S.M. McDeavitt, Thermophysical investigations of the uranium-zirconium alloy system. *J. Alloys Compd.* **611**, 355–362 (2014). <https://doi.org/10.1016/j.jallcom.2014.05.126>
- S.T. Ziegler, The uranium-rich end of the uranium-zirconium system, Argonne Natl. Lab Metall. Progr. 3.1.3. ANL-6055 (1962)
- H. Okamoto, U-zr (uranium-zirconium). *J. Phase Equilibria* **28**, 499 (1992). <https://doi.org/10.1007/BF02645399>
- K.H. Kim, S.J. Oh, S.K. Kim, C.T. Lee, C.B. Lee, Microstructural characterization of U-Zr alloy fuel slugs for sodium-cooled fast reactor. *Surf. Interface Anal.* (2012). <https://doi.org/10.1002/sia.4989>
- A.C. Lawson, C.E. Olsen, J.W. Richardson, M.H. Mueller, G.H. Lander, Structure of β -uranium. *Acta Crystallogr. Sect. B* **44**, 89–96 (1988). <https://doi.org/10.1107/S0108768187009406>
- M. Akabori, T. Ogawa, A. Itoh, Y. Morii, The lattice stability and structure of delta -UZr₂ at elevated temperatures. *J. Phys. Condens. Matter.* **7**, 8249–8257 (1995). <https://doi.org/10.1088/0953-8984/7/43/005>
- S. Irukuvarghula, S. Ahn, S.M. McDeavitt, Decomposition of the γ phase in as-cast and quenched U-Zr alloys. *J. Nucl. Mater.* **473**, 206–217 (2016). <https://doi.org/10.1016/j.jnucmat.2016.02.028>
- A.P. Moore, C. Deo, M.I. Baskes, M.A. Okuniewski, Atomistic mechanisms of morphological evolution and segregation in

- U-Zr alloys. *Acta Mater.* **115**, 178–188 (2016). <https://doi.org/10.1016/j.actamat.2016.05.052>
25. W.J. Williams, M.A. Okuniewski, L. Sudderth, D. Wachs, S. Van Den Berghe, Fabrication and characterization of U-Zr foils for the DISECT project. *Trans. Am. Nucl. Soc.* **118**, 348–351 (2018)
 26. W.J. Williams, C. Hale, E. Sikik, M. Sprenger, G. Borghmans, D.M. Wachs, S. van den Berghe, M.A. Okuniewski, T. Maddock, B. Boer, Thermal-hydraulics and neutronics overview of the DISECT experiment. *Trans. Am. Nucl. Soc.* **120**, 348 (2019)
 27. J.L. McDuffee, G.L. Bell, R.J. Ellis, R.W. Hobbs, M.A. Okuniewski, L.L. Snead, Design, Fabrication, and Testing of Gadolinium-Shielded Metal Fuel Samples in the Hydraulic Tube of the High Flux Isotope Reactor, in: *Water React. Fuel Perform. Meet. Fuel/LWR Fuel Perform. Meet.*, Sendai, Japan (2014), p. 100084
 28. M. Klinge, More features, more tools, more CrysTBox. *J. Appl. Crystallogr.* (2017). <https://doi.org/10.1107/S1600576717006793>
 29. E.E. Underwood, *Quantitative Stereology for Microstructural Analysis* (Springer, Boston, 1970)
 30. G.F. Vander Voort, A. Roósz, Measurement of the interlamellar spacing of pearlite. *Metallography* **17**, 1–17 (1984). [https://doi.org/10.1016/0026-0800\(84\)90002-8](https://doi.org/10.1016/0026-0800(84)90002-8)
 31. E.R. Boyko, The structure of the δ phase in the uranium–zirconium system. *Acta Crystallogr.* **10**, 712–713 (1957). <https://doi.org/10.1107/s0365110x57002492>
 32. H. Blank, Fractional packing densities and fast diffusion in uranium and other light actinides. *J. Alloys Compd.* **268**, 180–187 (1998). [https://doi.org/10.1016/S0925-8388\(97\)00604-X](https://doi.org/10.1016/S0925-8388(97)00604-X)
 33. C. Basak, G.J. Prasad, H.S. Kamath, N. Prabhu, An evaluation of the properties of As-cast U-rich U-Zr alloys. *J. Alloys Compd.* **480**, 857–862 (2009). <https://doi.org/10.1016/j.jallcom.2009.02.077>
 34. M. Kato, K. Morimoto, H. Sugata, K. Konashi, M. Kashimura, T. Abe, Solidus and liquidus temperatures in the UO_2 - PuO_2 system. *J. Nucl. Mater.* **373**, 237–245 (2008). <https://doi.org/10.1016/j.jnucmat.2007.06.002>
 35. A. Aitkaliyeva, J.W. Madden, C.A. Papesch, J.I. Cole, TEM identification of subsurface phases in ternary U-Pu-Zr fuel. *J. Nucl. Mater.* **473**, 75–82 (2016). <https://doi.org/10.1016/j.jnucmat.2016.02.022>
 36. Y. Xie, M.T. Benson, J.A. King, R.D. Mariani, J. Zhang, Characterization of U-Zr fuel with alloying additive Sb for immobilizing fission product lanthanides. *J. Nucl. Mater.* **498**, 332–340 (2018). <https://doi.org/10.1016/j.jnucmat.2017.10.039>
 37. D.E. Janney, T.P. O'Holleran, Zr inclusions in actinide-Zr alloys: New data and ideas about how they form. *J. Nucl. Mater.* **460**, 13–15 (2015). <https://doi.org/10.1016/j.jnucmat.2015.01.065>
 38. D.E. Janney, J.R. Kennedy, J.W. Madden, T.P. O'Holleran, Crystal structure of high-Zr inclusions in an alloy containing U, Pu, Np, Am, Zr and rare-earth elements. *J. Nucl. Mater.* **448**, 109–112 (2014). <https://doi.org/10.1016/j.jnucmat.2014.01.044>
 39. I. Manna, P.P. Chattopadhyay, F. Banhart, H.J. Fecht, Formation of face-centered-cubic zirconium, by mechanical attrition. *Appl. Phys. Lett.* **81**, 4136–4138 (2002). <https://doi.org/10.1063/1.1519942>
 40. H. Zhao, X. Hu, M. Song, S. Ni, Mechanisms for deformation induced hexagonal close-packed structure to face-centered cubic structure transformation in zirconium. *Scr. Mater.* **132**, 63–67 (2017). <https://doi.org/10.1016/j.scriptamat.2017.01.034>